

Mechanisms of Forced Tropical Meridional Energy Flux Change

SPENCER A. HILL

Program in Atmospheric and Oceanic Sciences, Princeton University, Princeton, New Jersey

YI MING AND ISAAC M. HELD

NOAA/Geophysical Fluid Dynamics Laboratory, Princeton, New Jersey

(Manuscript received 18 February 2014, in final form 20 May 2014)

ABSTRACT

Anthropogenically forced changes to the mean and spatial pattern of sea surface temperatures (SSTs) alter tropical atmospheric meridional energy transport throughout the seasonal cycle—in total, its partitioning between the Hadley cells and eddies and, for the Hadley cells, the relative roles of the mass flux and the gross moist stability (GMS). The authors investigate this behavior using an atmospheric general circulation model forced with SST anomalies caused by either historical greenhouse gas or aerosol forcing, dividing the SST anomalies into two components: the tropical mean SST anomaly applied uniformly and the full SST anomalies minus the tropical mean.

For greenhouse gases, the polar-amplified SST spatial pattern partially negates enhanced eddy poleward energy transport driven by mean warming. Both SST components weaken winter Hadley cell circulation and alter GMS. The Northern Hemisphere–focused aerosol cooling induces northward energy flux anomalies in the deep tropics, which manifest partially via strengthened northern and weakened southern Hadley cell overturning. Aerosol-induced GMS changes also contribute to the northward energy fluxes. A simple thermodynamic scaling qualitatively captures these changes, although it performs less well for the greenhouse gas simulations. The scaling provides an explanation for the tight correlation demonstrated in previous studies between shifts in the intertropical convergence zone and cross-equatorial energy fluxes.


1. Introduction

Earth absorbs more solar radiation in the tropics than at high latitudes, driving atmospheric circulations that transport energy poleward. This poleward flux occurs through the mean meridional circulation (MMC), stationary eddies, and transient eddies:

$$[\overline{mv}] = \underbrace{[\overline{m}][\overline{v}]}_{\text{MMC}} + \underbrace{[\overline{m^*v^*}]}_{\text{stationary eddies}} + \underbrace{[\overline{m'v'}]}_{\text{transient eddies}}, \quad (1)$$

where $m = c_p T + gz + L_v q$ is moist static energy (MSE),¹ overbars denote time means, primes denote deviations from the time mean, square brackets denote zonal means, asterisks denote deviations from the zonal mean, and notation is otherwise standard. In the tropics, the MMC consists of the two Hadley cells.

Both the total tropical atmospheric energy transport and its partitioning among these flow components vary with the seasonal cycle (e.g., [Trenberth and Stepaniak 2003](#)). The Hadley cells are the largest contributors in the deep tropics and primarily flux energy poleward, with the large winter cell spanning across the equator and including a flux from the summer to the winter hemisphere. Stationary eddy transports are also

 Denotes Open Access content.

Corresponding author address: Spencer Hill, NOAA Geophysical Fluid Dynamics Laboratory, 201 Forrester Rd., Princeton, NJ 08540.
E-mail: spencerh@princeton.edu

¹ Moist static energy neglects kinetic energy, which is rarely important for large-scale energy transport (e.g., [Trenberth and Stepaniak 2003](#)).

DOI: 10.1175/JCLI-D-14-00165.1

primarily poleward, and transient eddy poleward fluxes are large in autumn and winter, increasing in magnitude moving away from the equator. The dynamics controlling the Hadley cell strength and extent is also seasonal, the winter cell adhering more closely to the classical angular-momentum-conserving models (e.g., Held and Hou 1980), but with eddy stresses strongly affecting the circulation in the equinoctial and summer cells and the poleward flank of the winter cell (e.g., Salmon et al. 2001; Walker and Schneider 2006; Merlis et al. 2013a).

The fluxes of energy and mass by the Hadley cells are linked via the gross moist stability (GMS). As the Hadley cells overturn, their upper and lower branches transport energy in opposite directions so that the net meridional energy flux depends on their degree of compensation (Held and Hoskins 1985). This compensation depends on 1) the rate of mass circulation (known as the mass flux) and 2) the meridional energy flux per unit mass flux, which is the GMS. Symbolically at a given latitude ϕ ,

$$F_{\text{HC}}(\phi) = \Psi_{\text{max}}(\phi)\Delta_{\text{HC}}(\phi), \quad (2)$$

where F_{HC} is the energy flux by the Hadley cells, Ψ_{max} the mass flux, and Δ_{HC} the GMS. This expression in fact defines GMS as the ratio of the Hadley cell energy flux to the mass flux;² in this sense GMS can be thought of as the efficiency of meridional energy transport by the Hadley cells.

It follows from Eq. (2) for sufficiently small perturbations that fractional changes in these quantities are related by

$$\frac{\delta F_{\text{HC}}(\phi)}{F_{\text{HC}}(\phi)} = \frac{\delta \Psi_{\text{max}}(\phi)}{\Psi_{\text{max}}(\phi)} + \frac{\delta \Delta_{\text{HC}}(\phi)}{\Delta_{\text{HC}}(\phi)}. \quad (3)$$

Merlis et al. (2013a) show that, at the Hadley cell centers in an intermediate complexity aquaplanet model forced by orbital precession changes, GMS can overcompensate for the imposed meridional energy imbalance, such that the fractional mass and energy flux changes are of opposite sign. Merlis et al. also find the GMS response to be captured by a simple approximation by Held (2001, hereafter H01) relating GMS to the surface meridional MSE gradient.

Meridionally asymmetric energy perturbations—for example, the Northern Hemisphere-centric anthropogenic aerosols or asymmetric feedbacks to the more

uniform greenhouse gas forcing—can push the inner boundary of the Hadley cells, and with it the intertropical convergence zone (ITCZ), farther away from the energy deficient hemisphere (e.g., Kang et al. 2008, 2009; Ming and Ramaswamy 2011; Chiang and Friedman 2012; Frierson and Hwang 2012). This meridional shift manifests as a spinup of the cell in the energy-excessive hemisphere and a spindown in the energy-deficient one. If GMS change compensates for some of the induced energy imbalance, then by Eq. (3) the mass circulation response—and with it the ITCZ shift—will be weaker. Yet prior studies have found changes in the ITCZ position to be tightly correlated with anomalous atmospheric energy transport at the equator (Frierson and Hwang 2012; Donohoe et al. 2013), suggesting a modest role for GMS change in and of itself near the cells' shared equatorward border.

Several other recent studies have investigated GMS in the context of meridional energy transports and movement of the ITCZ (e.g., Frierson 2007; Kang et al. 2009; Kang and Held 2012; Merlis et al. 2013b,c), but all use zonally symmetric aquaplanet models [or a simple zonally symmetric continent in Merlis et al. (2013b)], often with simplified treatments of radiation, convection, and other relevant processes. The behavior of tropical moist stability in global warming has also been studied more generally, with stability changes fundamental to the “up-ped-ante” and “rich-get-richer” mechanisms of Neelin et al. (2003) and Chou and Neelin (2004).

The role of sea surface temperatures (SSTs) in tropical dynamics has long been appreciated. The ITCZ in axisymmetric models is collocated with the near-surface MSE maximum (Privé and Plumb 2007), itself strongly dependent on SSTs. Deep convection in the ITCZ effectively communicates surface conditions all the way to the tropopause and nearly homogenizes the column MSE. The weak temperature gradient constraint aloft (e.g., Sobel et al. 2001) can then effectively communicate this to the whole tropical free troposphere. Moreover, anthropogenic forcing can alter the tropical circulation and precipitation via changing the mean (e.g., Held and Soden 2006) and spatial pattern (e.g., Xie et al. 2013) of SSTs.

These considerations compel us to study how anthropogenically forced changes to the SST field—both its mean and its spatial pattern—alter the tropical meridional energy flux throughout the seasonal cycle in a comprehensive atmospheric general circulation model (AGCM). Section 2 and the appendix describe our methodology. Section 3 presents the results of these prescribed SST simulations and a thermodynamic scaling for GMS change that builds on the ideas of H01. Discussion and summary follow in sections 4 and 5, respectively. We view these simulations as a bridge between the aforementioned idealized aquaplanet simulations and fully coupled GCMs (or the real world) in

² The HC subscript on the gross moist stability term is meant to emphasize that the energy flux is by the Hadley cells only. The analogous quantity that also includes eddy energy transports is known as “total GMS” (e.g., Kang et al. 2009). Moreover, gross moist stability can be defined in other ways than the zonal-mean, meridional flux form we use here, such as using the flux divergence (e.g., Neelin and Held 1987) or vertical velocity profile (e.g., Chou et al. 2009), in which cases it is a function of both longitude and latitude.

which such a decomposition of surface conditions into mean and spatial pattern components is not feasible.

2. Methods

a. Prescribed SST experiments

We first create SST anomalies representative of the effects of either forcing agent using the experiments of [Ming and Ramaswamy \(2009\)](#) with the Geophysical Fluid Dynamics Laboratory (GFDL) atmospheric GCM version 2.1 (AM2.1) ([Anderson et al. 2004](#); [Delworth et al. 2006](#)), with 2° latitude \times 2.5° longitude resolution, coupled to a 50-m mixed layer (or “slab”) ocean. The AGCM accounts for aerosol–cloud interactions via a prognostic cloud droplet number concentration scheme for shallow cumulus and stratiform clouds that depends on local aerosol concentrations ([Ming et al. 2006, 2007](#)). A control case with preindustrial atmospheric composition is perturbed with preindustrial to present-day anthropogenic burdens of either well-mixed greenhouse gas or aerosols. We run the preindustrial control, present-day greenhouse gas, and present-day aerosol cases to equilibrium, averaging the annual cycle of SSTs over model years 61–80 to produce a climatological SST annual cycle. We then subtract the control from the perturbation SSTs to obtain a SST anomaly field for each forcing agent.

Next, we add these SST anomalies to observed climatological SSTs from the NOAA Optimal Interpolation (OI) sea surface temperature dataset ([Reynolds et al. 2002](#)) averaged over 1981–2005, again retaining an annual cycle. These SST fields along with observed climatological sea ice are then used to drive AM2.1, with the same annual cycle repeated each year. This yields a control case and greenhouse gas and aerosol perturbation cases. The AGCM is run for 17 years, with the first year discarded as spinup and results averaged over the subsequent 16. Results averaged over the first 8 yr or subsequent 8 yr of the averaging period are largely similar to results using all 16. Unless otherwise noted, all subsequent discussion of results is for the prescribed SST experiments.

Two additional simulations for each forcing agent isolate the roles of changes to the mean and spatial pattern of SSTs. In the first, the annual mean SST change averaged over the tropics ($+2.0$ K for greenhouse gases, -1.1 K for aerosols; tropics defined as 30°S – 30°N) is added to the climatology at every ocean grid point and time step.³ In the second, this tropical mean SST change

is subtracted from the full SST anomaly field at each ocean grid point before being added to the climatology. These experiments thus represent the mean temperature change and spatial pattern components, respectively. [Ma and Xie \(2013\)](#) perform an analogous decomposition into mean and spatial pattern components in the Community Atmosphere Model version 3 (CAM3) AGCM in their analysis of circulation and precipitation responses to anthropogenic forcing.

The near-zero tropical mean temperature change in the spatial pattern simulations negates changes in specific humidity induced via the Clausius–Clapeyron relation. Changes in annual and tropical mean water vapor path are -0.1 and -0.2 kg m^{-2} for the spatial pattern cases of greenhouse gases and aerosols, respectively, compared to $+6.9$ and -3.2 kg m^{-2} for the mean temperature change components and $+6.7$ and -3.4 kg m^{-2} for the full perturbation cases. In this sense, the mean and spatial pattern cases can be roughly thought of as the “thermodynamic” and “dynamic” components of the total response to the anomalous SSTs. The atmosphere responds quite linearly to the mean/spatial pattern decomposition, in that for all quantities analyzed the response to the full perturbation roughly equals the sum of the responses in the corresponding mean temperature change and spatial pattern cases (shown below for the energy flux).

b. Treatment of direct radiative forcing and surface fluxes

The atmospheric composition in all prescribed SST experiments is present day. Therefore, any differences in the climate response stem solely from differences in the imposed SST fields, and fast atmospheric adjustments (in particular by clouds) to the forcing agent are only incorporated to the extent that they affect the SST field in the original slab-ocean experiments. Nevertheless, the total atmospheric energy flux, mass flux, and GMS are to first order identical in the mixed layer ocean–AM2.1 and prescribed SST configurations (not shown), suggesting that fast atmospheric adjustments that do not imprint onto the SST field are of secondary importance for the large-scale energetic response. The mixed layer ocean simulations include prescribed ocean surface flux adjustments as standard to mimic ocean heat transport. There are no prescribed surface fluxes in the prescribed SST simulations.

Altered atmospheric MSE transport is not the sole possible means of adjustment to an imposed meridionally asymmetric forcing: ocean heat transport or local radiative adjustments (e.g., via clouds) are feasible alternatives and are recognized to affect the ITCZ position (and hence the cross-equatorial energy flux) (e.g., [Kang et al. 2008, 2009](#); [Frierson and Hwang 2012](#); [Frierson et al. 2013](#); [Marshall et al. 2014](#)). Also, as

³ By coincidence of the tropical mean greenhouse gas warming being just under 2 K, the mean warming case is essentially identical to commonly run “plus 2 K” or “Cess” uniform SST warming simulations.

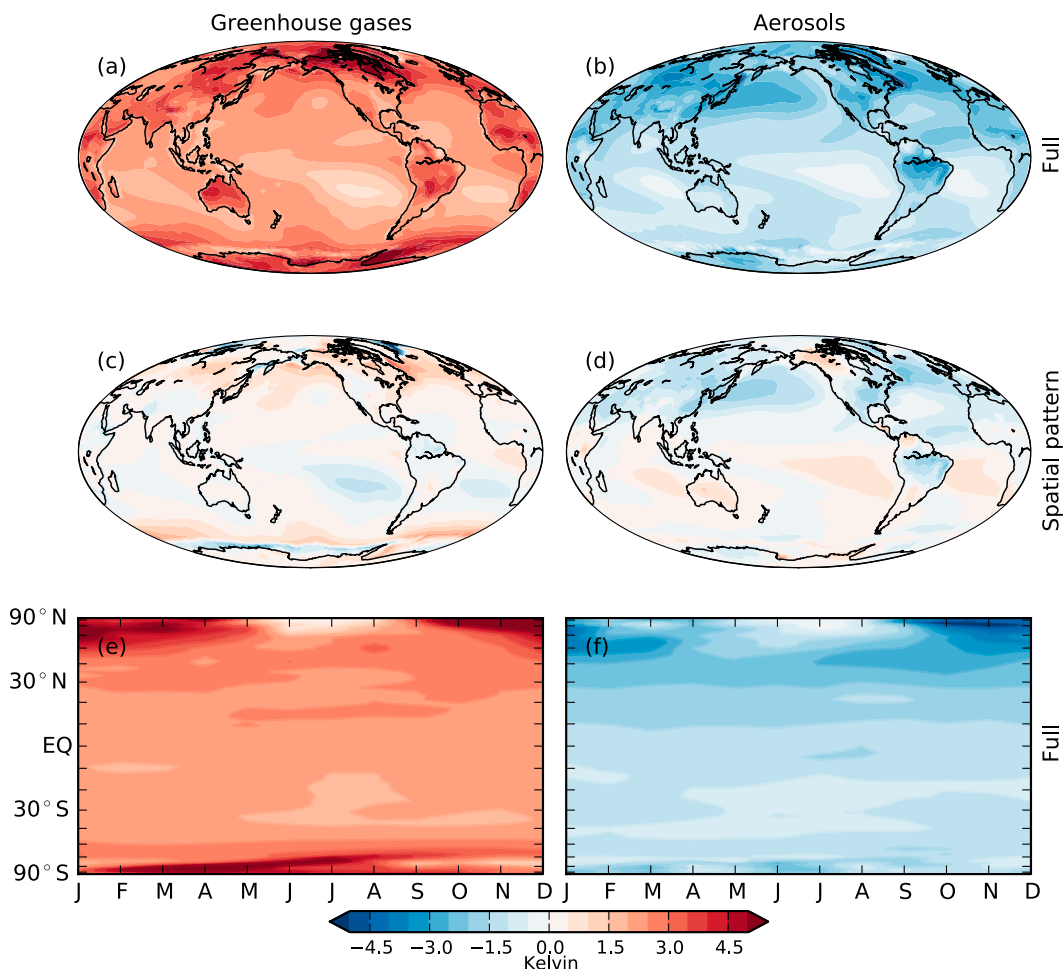


FIG. 1. Surface air temperature response for the prescribed SST experiments: annual mean for (a) greenhouse gases, (b) aerosols, (c) greenhouse gas spatial pattern, and (d) aerosol spatial pattern, and the annual cycle of their zonal mean for (e) greenhouse gases and (f) aerosols. The vertical axis in (e) and (f) is $\sin\phi$ to be proportional to the earth's fractional surface area at each latitude.

demonstrated by Yoshimori and Broccoli (2008) and Frierson and Hwang (2012), cross-equatorial energy transports are ultimately tied to the top-of-atmosphere (TOA) radiative imbalance between the hemispheres, for which the hemispheric mean surface temperature is a good, but not perfect, indicator. Kang and Held (2012) demonstrate SSTs to be a similarly imperfect proxy for surface energy fluxes in driving tropical precipitation anomalies. Our focus on atmospheric MSE transports and framing of the energy transports and precipitation as responding to SST perturbations should be interpreted with these caveats in mind.

The appendix details how the energy flux, mass flux, and gross moist stability are calculated, including the partitioning of the energy flux among the MMC, stationary eddy, and transient eddy terms, a simple adjustment based on mass balance considerations applied in the MMC energy flux computation, and the sensitivity of the energy flux calculations to the height of the vertical integral.

3. Results

a. Surface temperature

Figure 1 shows the annual mean latitude–longitude pattern of surface air temperature change for the full and spatial pattern perturbation cases of each forcing agent. Tight coupling of the ocean and near-surface atmosphere causes these values over ocean to be nearly identical to the imposed SSTs (not shown), except for high-latitude locations where the prevailing meteorology decouples the atmosphere from the surface. Table 1 lists the global mean, tropical mean, and Northern Hemisphere (NH) minus Southern Hemisphere (SH) annual mean surface air temperature responses for each perturbation simulation. Warming by greenhouse gases and weaker cooling by aerosols are evident (+2.6 and −1.6 K global mean, respectively), as are the polar amplified

TABLE 1. Annual mean surface air temperature anomaly (in K) for the global mean, the tropics (30°S–30°N), and the Northern Hemisphere minus the Southern Hemisphere in the full, mean, and spatial pattern simulations for greenhouse gases and aerosols.

	Globe	Tropics	NH – SH
Greenhouse gases			
Full	2.6	2.3	0.3
Mean	2.3	2.3	0.1
Spatial pattern	0.1	–0.1	0.2
Aerosols			
Full	–1.6	–1.3	–0.9
Mean	–1.3	–1.3	–0.1
Spatial pattern	–0.3	–0.1	–0.7

spatial pattern of the greenhouse gases and the aerosol-induced cooling of the NH relative to the SH (NH and SH mean change are +2.7 and +2.4 K respectively for greenhouse gases and –2.0 and –1.1 K for aerosols).

Figure 1 also shows the annual cycle of the zonal mean surface air temperature change for both full cases. The weakest changes occur in the Arctic during NH summer when melting ice and snow peg surface temperature to the freezing point. Both also have their maximum magnitudes in the Arctic during winter, as the prevailing near surface inversion inhibits turbulent fluxes, thereby forcing the energetic anomalies to be shed via changes in longwave emission (e.g., Boé et al. 2009; Lesins et al. 2012). This results in seasonal variations in the NH high-latitude surface temperature response of ~6 K for greenhouse gases and ~4 K for aerosols, in contrast to $\lesssim 1$ K in the tropics for either forcing agent.

b. Energy flux

Figure 2 shows the annual cycle of the monthly mean meridional energy flux in total and for the three flow components in the control experiment. Outside ~20°S–20°N, transport is poleward in both hemispheres year-round, reaching peak magnitudes near 7 PW in the midlatitudes in early winter. The Hadley cells contribute up to ~3 PW in mid to late winter of either hemisphere. Stationary eddies contribute up to ~3 PW to the poleward transport in the NH midlatitudes in winter, but their contribution in the tropics is weaker. Transient eddies contribute more than 5 PW to the poleward energy transport in autumn and winter over much of the midlatitudes, with spillover of up to 4 PW extending through the tropics.

Gray curves in this and subsequent figures indicate the locations of the Hadley cell boundaries, calculated as the zero crossings of the 500-hPa meridional mass streamfunction, linearly interpolating between the grid latitudes at which the streamfunction changes sign. As Dima and Wallace (2003) demonstrate for reanalysis

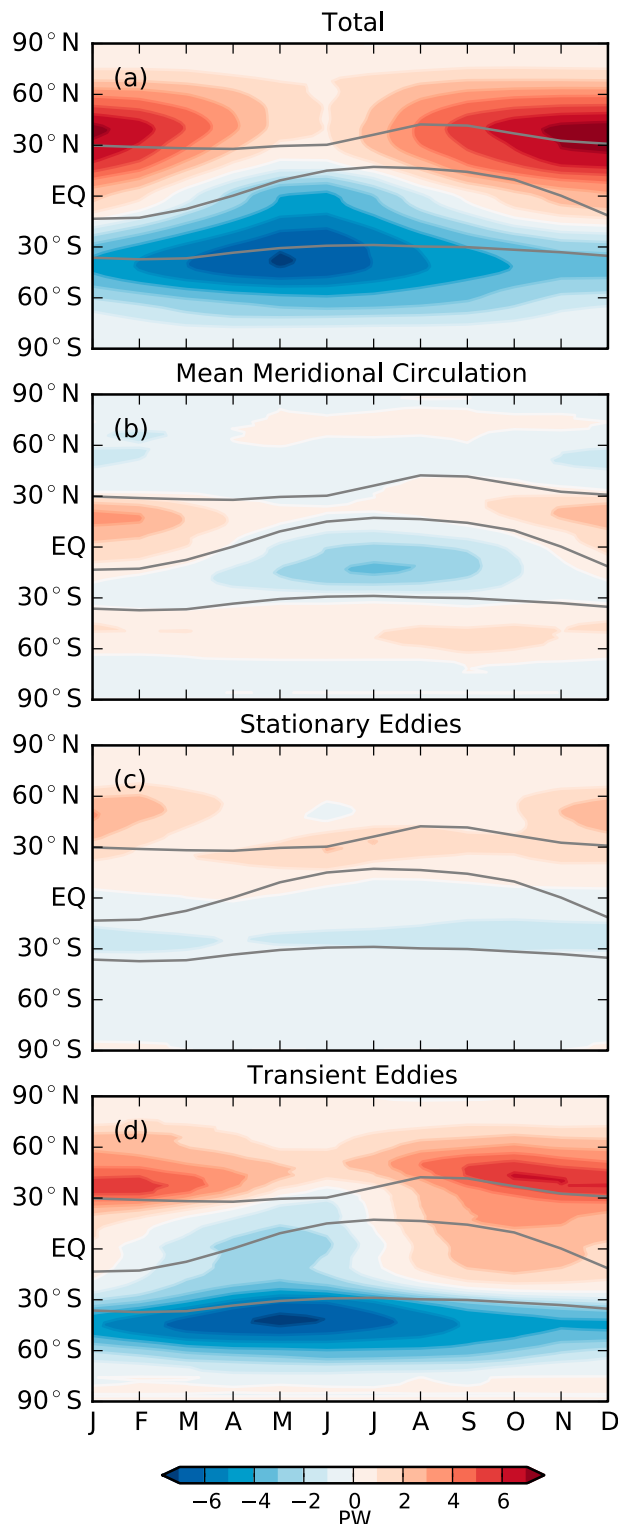


FIG. 2. Annual cycle of northward energy flux in the prescribed SST control simulation in color contours: (a) its total and contributions from (b) the mean meridional circulation, (c) stationary eddies, and (d) transient eddies. The appendix describes how these are calculated. Gray curves denote the positions of Hadley cell boundaries as defined by the zero crossings of the meridional mass streamfunction at 500 hPa. Because the flux calculations incorporate surface area, no $\sin\phi$ spacing is necessary on the vertical axis.

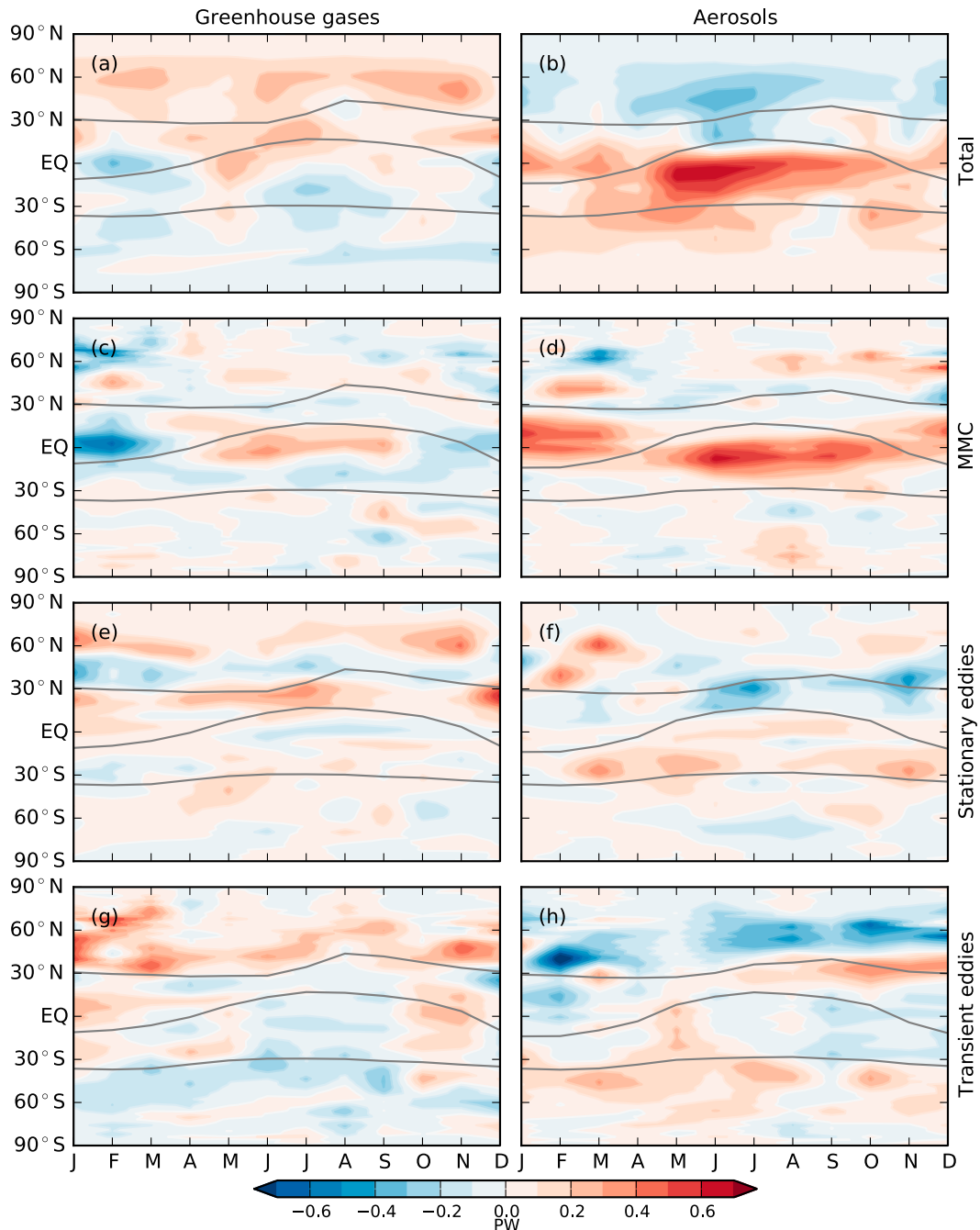


FIG. 3. Annual cycle of the anomalous northward atmospheric energy transport for the full (left) greenhouse gas and (right) aerosol simulations (a),(b) in total and by each flow component: (c),(d) the mean meridional circulation, (e),(f) stationary eddies, and (g),(h) transient eddies. Overlaid gray curves mark the locations of the Hadley cell boundaries in the perturbation simulation, as defined by the zero crossings of the meridional mass streamfunction at 500 hPa.

data, the two cells smoothly vary throughout the year between equinoctial and solstitial patterns (rather than displaying “square wave” behavior dominated by the solstitial cell as has sometimes been posited).

Figure 3 shows the total anomalous energy flux and the contributions of each flow component for the full

greenhouse gas and aerosol experiments; the overlaid Hadley cell boundaries are of the perturbation run. Greenhouse gases mostly increase poleward transport, with maximum magnitudes of ~ 0.4 PW. This is driven by eddies, with stationary eddies contributing northward anomalies over much of the NH tropics and transient

eddies enhancing poleward energy transport over most of the extratropics. In contrast, the Hadley cells tend to oppose this enhanced poleward transport, contributing southward anomalies in the NH winter cell up to -0.6 PW and northward anomalies in the SH winter cell up to $+0.4$ PW. These anomalous cross-equatorial fluxes likely stem from the seasonally reversing anomalous meridional temperature gradient: the minimum in Arctic warming and concurrent relative maximum Antarctic warming in boreal summer induce a northward cross-equatorial energy transport, and vice versa for austral summer.

Aerosols yield northward anomalies in the deep tropics year-round. They are centered on the equator, reach $+0.7$ PW in the SH winter cell, and occur almost exclusively via the Hadley cells. Interestingly, in the NH they are strongest in summer when Arctic cooling is minimum, rather than winter when the meridional gradient in temperature change is largest. Outside this region of strong northward anomalies, the picture is generally reduced poleward flux, with equatorward anomalies in either hemisphere. Stationary eddies contribute substantially to this weakening in the SH tropics, while transient eddies drive the extratropical response.⁴

Some latitudes and months exhibit pronounced repartitioning among the flow components despite weak change in the total flux. For example, the strongest anomalies in any field are for the aerosol transient eddies in February in the NH midlatitudes, with values reaching -0.8 PW. However, moderate northward anomalies in both the MMC and stationary eddy fields compensate, yielding only a -0.1 PW anomaly in the total flux.

Figure 4 shows the change in total atmospheric energy transport for the mean and spatial pattern cases of each forcing agent and their sum. For greenhouse gases, these components generally oppose each other. The mean warming enhances poleward energy transport via increased poleward moisture transport (not shown) (Manabe and Wetherald 1975; Held and Soden 2006; Hwang and Frierson 2010), with magnitudes near 0.3 PW for much of the year in the subtropics. In contrast, the polar amplified spatial pattern reduces the meridional temperature gradient, thereby weakening the poleward flux. The former effect being stronger than the latter in this case, the net result is enhanced poleward energy transport that is weaker than the mean warming case (Caballero and Langen 2005).

Aerosol mean cooling weakens the poleward energy flux by more than 0.2 PW at most latitudes/months via

the same moisture flux mechanism (albeit with opposite sign) as the greenhouse gas mean warming case. Meanwhile, the aerosol spatial pattern drives the strong northward anomalies (up to $+0.7$ PW) in the deep tropics apparent in the full case. These anomalies are strongest just poleward of the Hadley cells' interior boundary in either hemisphere. Thus the mean and spatial pattern effects buttress one another in the southern Hadley cell but oppose each other in the northern cell, resulting in the full aerosol case in northward anomalies that peak in the SH winter cell just south of the cells' shared border.

Combining these two decompositions—into MMC/stationary eddy/transient eddy components of the energy flux and into mean/spatial pattern of SSTs—the following picture emerges: greenhouse gas warming enhances poleward energy transport mostly through eddies, an effect that is partially negated by the weakened meridional temperature gradient. Meanwhile, the aerosol spatial pattern of relative NH cooling induces northward anomalies in the deep tropics that occur via the Hadley cells and are superimposed on reduced poleward energy transport owing to the mean cooling. Comparing the sum of the mean and spatial pattern components (Figs. 4e,f) to the full case (Figs. 3a,b) reveals that the response is quite linear to the imposed decomposition for either forcing agent.

c. Mass flux

That the Hadley cells contribute nonnegligibly for greenhouse gases and substantially for aerosols to the anomalous energy flux justifies analysis of the relative roles of both the mass flux and gross moist stability, starting with the mass flux Ψ_{\max} . We define Ψ_{\max} conventionally (see the appendix) as the signed maximum magnitude of the Eulerian mean meridional streamfunction Ψ at each latitude, such that positive values correspond to northward flow aloft as in the NH cell. Therefore, Ψ_{\max} is climatologically the same sign as the energy flux F_{HC} .

Figure 5 shows the mass flux annual cycle in the control for 45°S – 45°N . Values peak in the winter cells and are strongly seasonal in the deep tropics, ranging from $15 \times 10^{10} \text{ kg s}^{-1}$ in January to $-24 \times 10^{10} \text{ kg s}^{-1}$ in July. This seasonality weakens moving toward the subtropics: at 30°S/N the mass flux is of the same sign year-round, with an annual range of $\sim 4 \times 10^{10} \text{ kg s}^{-1}$.

Figure 6 shows the mass flux response annual cycle in the six perturbation experiments. Changes of substantial magnitude are bounded by the extent of the Hadley cell interior boundary seasonal migration, $\sim 15^{\circ}\text{S}$ – 15°N , hinting that the Hadley circulation responds primarily via alterations to its interior boundary location. For greenhouse gases the interior boundary moves southward April through September and northward otherwise, whereas for

⁴ Although MSE flux anomalies by eddies in the deep tropics are weak in our simulations, the possible significance of eddy MSE fluxes there cannot, in general, be discounted—Fig. 2 demonstrates this for the climatology (see also Peters et al. 2008).

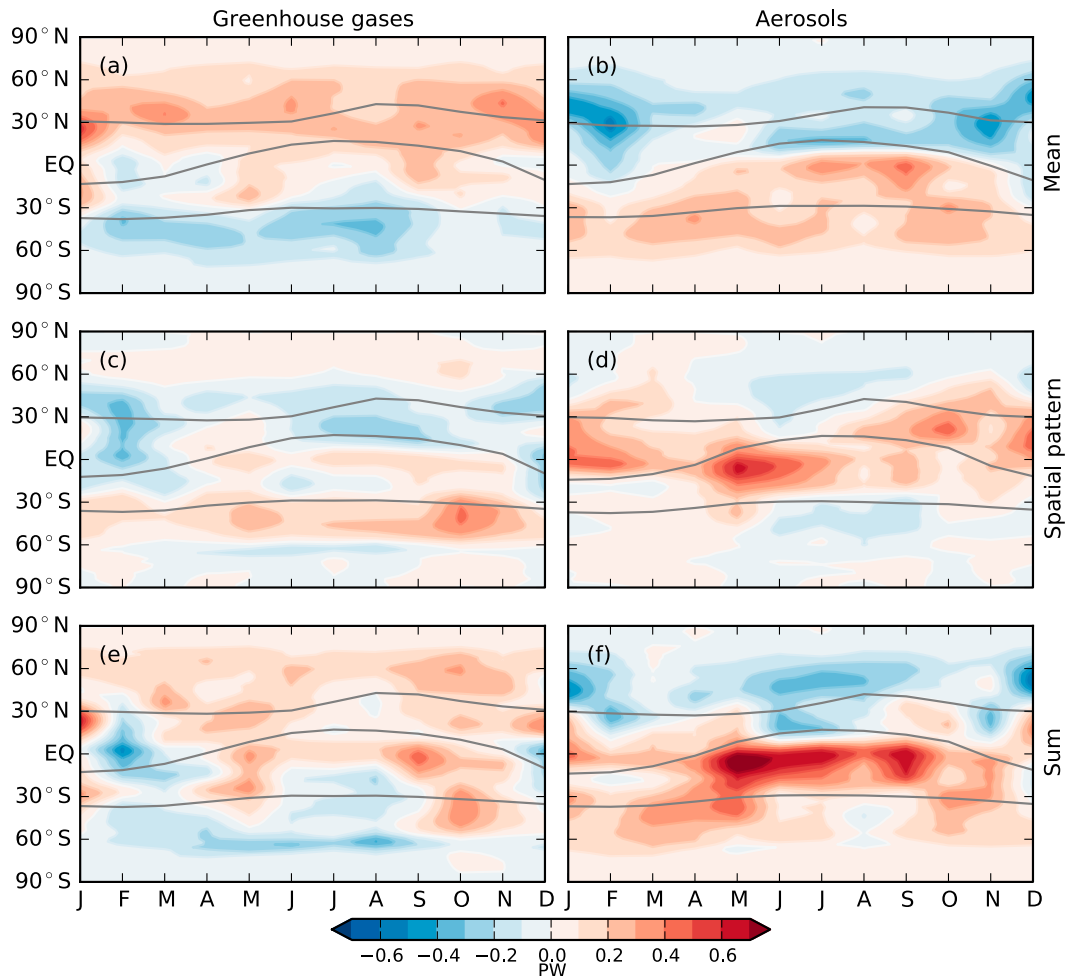


FIG. 4. As in Fig. 3, but for anomalous total northward atmospheric energy transport, as defined by Eq. (A4) for the (top) uniform temperature change simulation, (middle) spatial pattern simulation, and (bottom) their sum. The gray curves denote the (a)–(d) Hadley cell borders in the perturbation simulation and (e), (f) the average of their values in the uniform and spatial pattern simulations.

aerosols it moves southward year-round—in both cases agreeing with the sign of the mass flux changes.

For greenhouse gases, the mass flux anomalies vary seasonally as to oppose the climatology, in the northern winter cell up to $-5.4 \times 10^{10} \text{ kg s}^{-1}$ and in the southern winter cell up to $3.6 \times 10^{10} \text{ kg s}^{-1}$. Kang et al. (2013) likewise see weakening of both winter cells in a 40-member ensemble of the Community Climate System Model, version 4 (CCSM4) GCM subject to A1B emissions scenario radiative forcing (which is dominated by increased greenhouse gas concentrations).

By coincidence, the mass flux responds similarly to the mean warming and spatial pattern components of greenhouse gas SSTs, both acting primarily against the climatology. For mean warming, we expect the total convective mass flux to decrease because the specific humidity increases faster with temperature than the

precipitation (Knutson and Manabe 1995; Held and Soden 2006). If not constrained by other factors, one expects the mean meridional overturning mass flux to participate in this reduction, as seen here. (Being equatorward of 15° latitude, the large changes in seasonal Hadley cell mass flux are unlikely constrained by eddy momentum fluxes through the small-Rossby-number zonal force balance between eddy momentum fluxes and Coriolis force.) For the polar amplified spatial pattern, the reduced meridional temperature gradient necessitates weaker poleward energy fluxes as discussed above. This is partly accomplished in the deep tropics via a weakening of the mass flux in the winter cell. The net result of these mechanisms is a stronger weakening of the circulation in total for greenhouse gases than for either the mean or spatial pattern component alone.

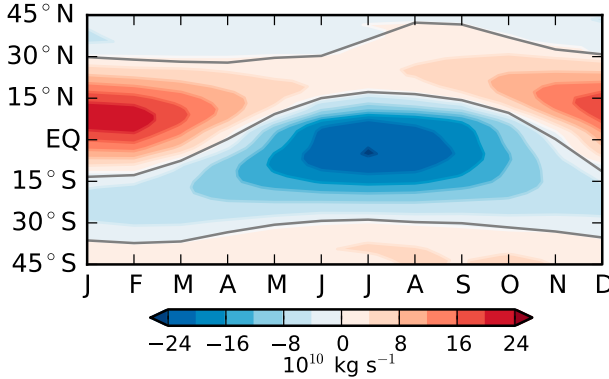


FIG. 5. Annual cycle of the mass flux, Ψ_{\max} , in the control simulation for 45°S–45°N, defined as the signed maximum magnitude of the meridional mass streamfunction at each latitude, where the streamfunction Ψ is defined as standard by Eq. (A5). Positive values, as in the NH cell, denote northward flow in the upper branch of the overturning circulation. Overlaid gray curves denote the boundaries of the Hadley cells defined based on the zero crossings of Ψ at 500 hPa.

Aerosols induce strong anomalies nearly year-round in the deep tropics, with maximum values in January through March near $+6 \times 10^{10} \text{ kg s}^{-1}$. These reinforce the climatology in the NH cell but counteract it in the SH cell and are collocated with the strong northward energy flux anomalies (Fig. 3). In other words, the spinup of the NH cell enhances the climatological northward energy flux, while the spindown of the SH cell weakens the climatological southward energy flux in that cell. Both cases yield anomalous northward energy fluxes.

The mean cooling contributes weakly to this pattern, with substantial anomalies (up to $-3.4 \times 10^{10} \text{ kg s}^{-1}$) only in July through September just south of the Hadley cells' shared border. The mean cooling of aerosols does not spin up the circulation in a scaled mirror image of the greenhouse gas mean warming; that is, the mass flux changes with uniform SST change are not symmetric about zero. This behavior is still under investigation. Wyant et al. (2006) demonstrate asymmetric tropical changes in both shortwave and longwave cloud radiative forcings in plus-2K and minus-2K experiments conducted in AM2.1, attributing them to differing condensate responses in ascent regions. Interestingly, they find no such asymmetry in another AGCM [i.e., the National Center for Atmospheric Research (NCAR) Community Atmosphere Model version 3.0 (CAM3.0)].

Nevertheless, the mean temperature change component contributes only weakly to the total aerosol mass flux response. Instead, the spatial pattern component drives the northward anomalies. This is consistent with the net northward energy flux anomalies (Fig. 3b) being driven by the spatial pattern simulation as well (Fig. 4d), as discussed previously.

d. Gross moist stability

As detailed in the appendix, we use a definition of GMS that includes only the Hadley cell contribution to the meridional energy flux, in order to understand the Hadley cell energy flux changes that dominate the total transport change for aerosols and the anomalous cross-equatorial MSE fluxes for greenhouse gases that oppose the enhanced poleward energy transport by eddies.

1) THEORY

We start with a simple estimate for GMS made by H01. Gross moist stability, as defined by Eq. (A6), is a meridional flow-weighted difference between upper-level and lower-level moist static energy (Neelin and Held 1987). In the limit of equal magnitude mass flow confined to one upper and one lower boundary layer, the mass flux weighting drops out and this simplifies to the upper-level minus lower-level MSE. At the ITCZ, deep convection homogenizes MSE vertically. Additionally, the weak temperature gradient dynamical constraint in the free troposphere horizontally homogenizes temperature and geopotential fields aloft. Together these imply that the surface MSE at the ITCZ sets the MSE field aloft throughout the tropics, and therefore GMS at a given latitude within the Hadley cells depends on the difference between surface MSE values locally and at the ITCZ:

$$\Delta_{\text{HC}}(\phi) \approx m_{\text{ITCZ}} - m(\phi), \quad (4)$$

where the subscript ITCZ denotes the value at the latitude of the ITCZ and MSE values are near surface.

H01 further simplifies by noting that geopotential is zero at the surface and writing $q = \mathcal{H}q_s$, where \mathcal{H} and q_s are the near-surface relative humidity and saturation specific humidity respectively, such that $m = c_p T + L_v \mathcal{H}q_s$. Then, neglecting meridional variations in \mathcal{H} , GMS becomes

$$\Delta_{\text{HC}}(\phi) \approx \left(c_p + L_v \bar{\mathcal{H}} \frac{dq_s}{dT} \bigg|_{\mathcal{H}} \right) [T_{\text{ITCZ}} - T(\phi)], \quad (5)$$

where $\bar{\mathcal{H}}$ is the tropical mean near-surface relative humidity and $dq_s/dT|_{\mathcal{H}}$ is the change in saturation specific humidity with respect to temperature at a fixed relative humidity, as governed by the Clausius–Clapeyron relation. Equation (5) states that GMS is determined solely by the meridional profile of surface temperatures and the tropical mean surface relative humidity. While H01 is concerned with the climatological annual mean GMS, Eqs. (4) and (5) are easily modified to represent GMS changes (e.g., between perturbation and control experiments). Merlis et al. (2013a) do so using Eq. (4), finding it to be a useful approximation of the GMS

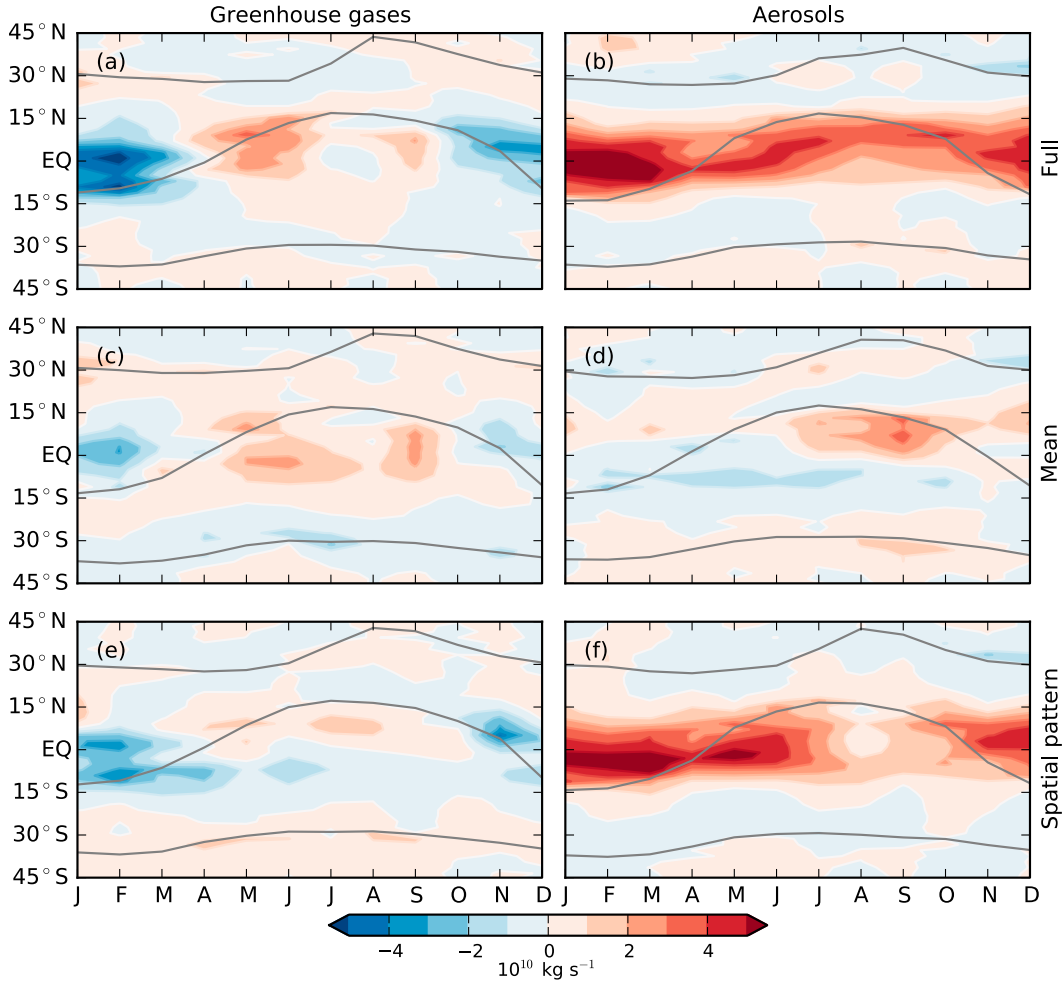


FIG. 6. Annual cycle of the mass flux response for 45°S–45°N in the (left) greenhouse gas and (right) aerosol (top) full, (middle) uniform temperature change, and (bottom) spatial pattern cases. Overlaid gray curves mark the locations of the Hadley cell boundaries in the perturbation simulation, as defined by the zero crossings of the meridional mass streamfunction at 500 hPa.

response to orbital precession in an idealized aquaplanet GCM (their Fig. 9).

We do likewise for our simulations but using a modified form of Eq. (5). Variations of relative humidity with latitude in the tropics for a given climate tend to exceed those at a given latitude in response to a climate perturbation. For example, annual and zonal mean relative humidity at 2 m above the surface varies by $\sim 15\%$ from the equator to 30° in either hemisphere in our control simulation, whereas the maximum magnitude change at a given tropical latitude from the control to any perturbation simulation is $\sim 1\%$. Therefore, we retain meridional variations in relative humidity and instead assume that specific humidity obeys the familiar thermodynamic scaling relation (i.e., $\delta q/q = \alpha \delta T$, where $\alpha = 7\% \text{ K}^{-1}$ represents the fractional increase in saturation vapor pressure with temperature via

Clausius–Clapeyron). With these alterations, the GMS change is given by

$$\delta \Delta_{\text{HC}}(\phi) = (c_p + \alpha L_v q_{\text{ITCZ}}) \delta T_{\text{ITCZ}} - [c_p + \alpha L_v q(\phi)] \delta T(\phi), \quad (6)$$

where δ denotes the difference between two climate states. Rearranging terms reveals the condition governing the sign of GMS change (the two equalities can be replaced with $>$ or $<$):

$$\delta \Delta_{\text{HC}}(\phi) = 0 \Leftrightarrow \frac{\delta T(\phi)}{\delta T_{\text{ITCZ}}} = \frac{c_p + \alpha L_v q_{\text{ITCZ}}}{c_p + \alpha L_v q(\phi)}. \quad (7)$$

Presumably $q_{\text{ITCZ}} > q(\phi)$, and therefore the rhs of the second equality in Eq. (7) is strictly greater than unity. Thus for GMS to remain constant, the magnitude of

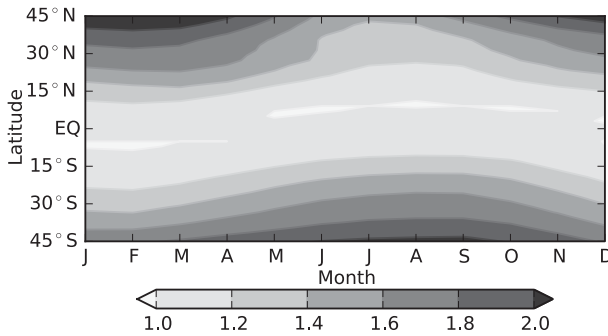


FIG. 7. Based on Eq. (7), the ratio of near-surface temperature change at the given latitude and at the intertropical convergence zone necessary for the GMS change to be zero. Here, 925-hPa values of q and T taken from the control simulation are used. The ITCZ latitude is taken as the latitude of maximum zonal mean precipitation, linearly interpolated between model grid points to where $\partial P/\partial \phi = 0$.

surface temperature change locally must exceed that at the ITCZ to an extent that depends on the existing specific humidity difference between them. Figure 7 shows this ratio $\delta T(\phi)/\delta T_{\text{ITCZ}}|_{\delta \Delta_{\text{HC}}=0}$ for the control experiment. As zonal mean specific humidity decreases monotonically away from the ITCZ into the subtropics (not shown), the temperature change ratio increases monotonically, reaching ~ 1.6 near the poleward boundaries of either Hadley cell.

For the particular case of a uniform δT , Eq. (6) reduces to $\delta \Delta_{\text{HC}}(\phi) = \alpha L_v [q_{\text{ITCZ}} - q(\phi)] \delta T$. Again assuming $q_{\text{ITCZ}} > q(\phi)$, the sign of the GMS change depends solely on the sign of δT . Uniform warming increases, and uniform cooling decreases, GMS at all latitudes outside the ITCZ, with the magnitude of the change increasing with the magnitude of the temperature change and moving toward the subtropics (we discuss the accuracy of this simple picture below). Given that climatologically GMS also increases meridionally away from ITCZ, this behavior in the case of uniform warming can be thought of as another manifestation of “rich-get-richer” behavior (Chou and Neelin 2004; Held and Soden 2006; Chou et al. 2009): the “stable get stabler” (taking liberty to define “the stable” as all latitudes outside the ITCZ).

2) RESULTS

Figure 8 shows the annual cycle of GMS in the control simulation. All GMS plots absorb a $1/c_p$ factor as standard to get units of Kelvin and have values outside of the Hadley cells masked. Overlaid in the blue dotted curve is the ITCZ location, defined as the latitude of maximum zonal mean precipitation, linearly interpolated from the model grid to the point where $\partial P/\partial \phi = 0$. The control GMS qualitatively adheres to the H01 picture, being

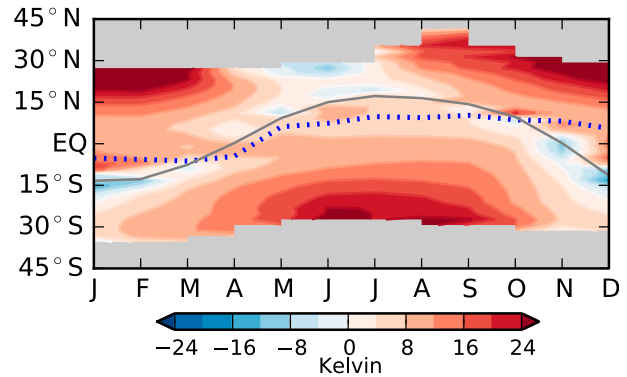


FIG. 8. Annual cycle of gross moist stability $\Delta_{\text{HC}}(\phi)$ in the control simulation. Positive values indicate that the net meridional energy flux is in the same direction as the flow in the upper branch, as occurs in the Hadley cells. Values outside the Hadley cells are masked, as the primary concern is with tropical energy fluxes and because the underlying dynamics differ markedly for the Hadley and Ferrel cells. The dotted blue line denotes the ITCZ location, taken as the latitude of maximum zonal mean precipitation, linearly interpolated between model grid points to where $\partial P/\partial \phi = 0$. GMS has been divided by c_p in this and all subsequent plots as standard to obtain units of Kelvin.

near zero following the boundary separating the Hadley cells and increasing poleward. However, the ITCZ is usually displaced equatorward from that border by several degrees latitude (Donohoe et al. 2013). Thus GMS at the ITCZ is generally positive (≥ 4 K), contradicting the Eq. (4) assertion that $\Delta_{\text{HC}} = 0$ at the ITCZ.

We discuss the GMS responses of the aerosol simulations first, being simpler than those of the greenhouse gas cases. Figure 9 shows the GMS response for the three aerosol cases (left column) and their corresponding estimates using Eq. (6) (right column). Values within 6° latitude of the Hadley cell interior border on either side are masked out for the full calculation, as it becomes problematic near where the mass flux goes to zero. The theoretical estimate uses values at 925 hPa. Despite its simplicity, Eq. (6) captures the qualitative behavior throughout the seasonal cycle in each simulation. For the full and spatial pattern cases, GMS decreases in the southern Hadley cell and increases in the northern cell for most of the year. For the uniform cooling simulation, the estimate features nearly monotonically decreasing GMS moving meridionally away from the convection zone. The actual response to uniform cooling (Fig. 9c) also predominantly features reductions, but with notable exceptions in the NH summer cell and over much of the year for $\sim 20^\circ$ – 30° S.

The spatial pattern component can also be understood via the theoretical estimate. Because the reduction in zonal mean surface temperature increases northward, GMS will decrease at latitudes south of the ITCZ and

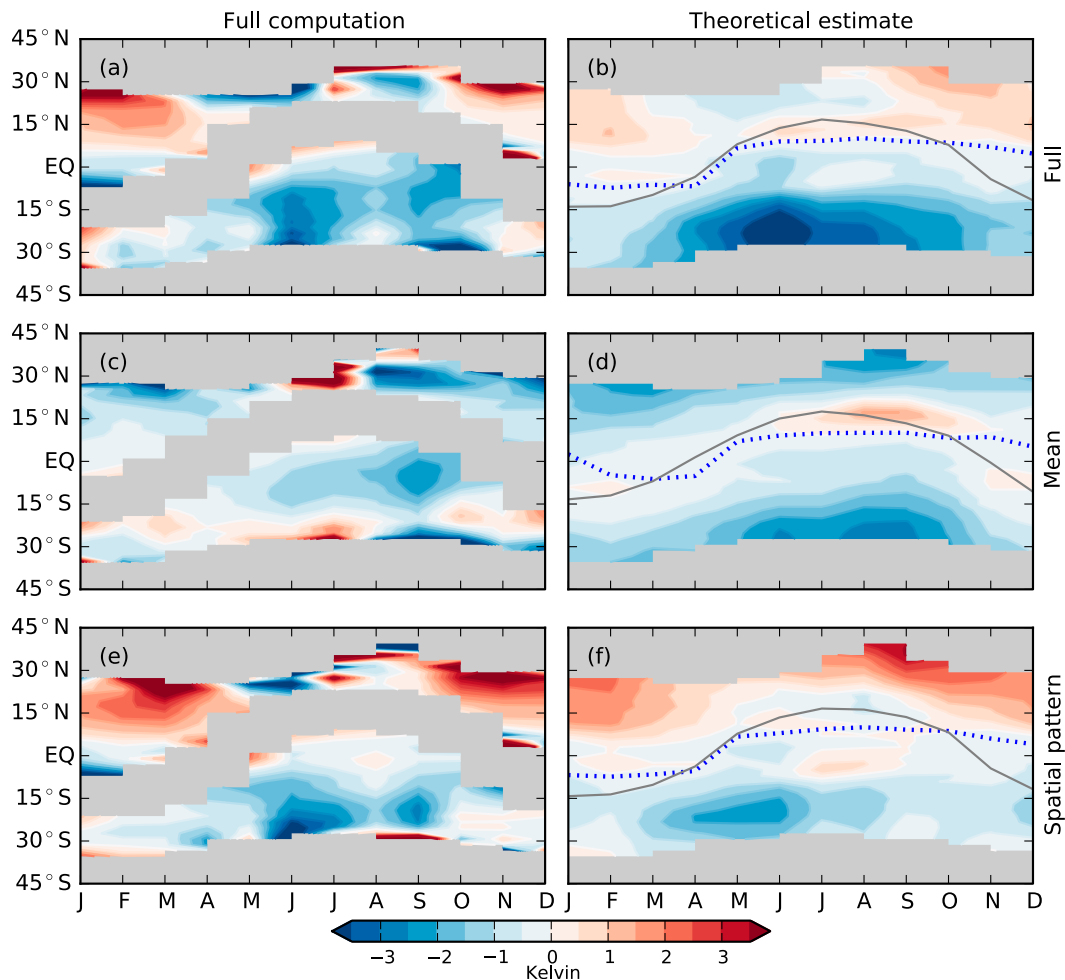


FIG. 9. Annual cycle of the gross moist stability response to the aerosol (top) full, (middle) uniform temperature change, and (bottom) spatial pattern cases, as computed using (left) the full GMS calculation of Eq. (A6) and (right) the theoretical estimate of Eq. (6). Values outside the Hadley cells are masked in all panels, and values within 6° latitude of the Hadley cell interior border (indicated by the thin gray curve in the right panels) on either side are also masked out in (left), as the GMS calculation becomes problematic near where the mass flux goes to zero. The Hadley cell boundaries are for the perturbation simulations, as defined by the zero crossings of the meridional mass streamfunction at 500 hPa. The dotted blue line denotes the ITCZ location in the perturbation simulation, taken as the latitude of maximum zonal mean precipitation, linearly interpolated between model grid points to where $\partial P/\partial \phi = 0$.

increase at latitudes north based on Eq. (7). This response yields an anomalous northward MSE transport that acts against the imposed cooling of the NH relative to the SH. Thus, as was the case with the MSE flux, the aerosol mean cooling and spatial pattern components reinforce each other in the southern Hadley cell and counteract each other in the northern cell, resulting in generally weaker GMS increases in the northern cell than decreases in the southern cell for the full aerosol case. This pattern of destructive versus constructive interference can also be seen in Table 2, which lists for each month in the full aerosol simulation the change in F_{HC} and the fractional changes in F_{HC} , Ψ_{max} , and Δ_{HC} at the latitude ϕ_{max} of the maximum magnitude of Ψ_{max} ,

which is essentially the center of the stronger Hadley cell. In the SH cell, more than half of the energy flux fractional change occurs via GMS, while the converse holds in the NH cell.

Figure 10 shows the GMS response for the three greenhouse gas cases and their corresponding Eq. (6) estimates. Equation (6) captures the qualitative behavior of GMS in the spatial pattern case: in the southern cell, slight decreases just south of the interior border most of the year and mild increases year-round south of $\sim 15^\circ\text{S}$ and, in the northern cell, mild decreases most of the year. This behavior is essentially a weakened mirror image of the aerosol spatial pattern case, as the zonal mean surface temperature response increases (becomes

more positive) nearly monotonically moving northward throughout the tropics. It acts to produce anomalous southward energy flux anomalies in either cell, consistent with the slight warming of the NH relative to the SH (Table 1).

The GMS responses to the full and uniform warming greenhouse gas cases are of comparable magnitude to the corresponding aerosol simulations but noisy, with Eq. (6) doing a much poorer job than for the spatial pattern or for the three aerosol cases. Note that GMS response to the uniform warming case is the only field featuring substantial variations between the two 8-yr averaging subperiods mentioned previously (not shown).

Two factors contribute to this discrepancy. First, MSE increases aloft at the ITCZ are smaller than at the surface year-round as a result of slight increases in boundary layer relative humidity (not shown), leading to an overestimate of GMS change when estimating the upper-level change in MSE at the ITCZ using the surface change at fixed relative humidity. Second, the weak temperature gradient approximation is imperfect; increases in MSE aloft are maximum in each month near the equator and become smaller monotonically moving poleward, albeit weakly (not shown). Combined, these effects lead to a more positive prediction of GMS change when using surface MSE differences [i.e., Eq. (6)] rather than local vertical MSE differences. Why these assumptions fail only in response to greenhouse gas full or uniform SSTs remains an open question.

4. Discussion

a. Implications of GMS change for forced ITCZ shifts

Equation (6) states that changes in GMS depend only on two fields: the climatological near-surface specific humidity and the anomalous surface temperature. Both quantities have some finite scale of meridional variations—Figs. 1e and 1f roughly indicate this for surface temperature anomalies. At latitudes sufficiently far away from the ITCZ, the differences relative to the ITCZ of either field can be substantial, and hence GMS can vary via thermodynamic scaling. But there exist latitudes that are too near the ITCZ to experience substantial differences in either field relative to their values at the ITCZ. As such, Eq. (6) states that GMS will not vary substantially at these latitudes by simple thermodynamic scaling behavior. As a result, anomalous energy fluxes must manifest exclusively via anomalous circulation, consistent with large mass flux changes being confined to the latitudes near the ITCZ (Fig. 6).

We speculate that this explains why the ITCZ position has been found to be so tightly correlated with atmospheric energy transport at the equator (e.g., Frierson and Hwang 2012; Donohoe et al. 2013): near the equator, dynamical shifts of moisture convergence are the only practical means by which to substantially alter the energy transport. Moreover, latitudes near the energy transport zero-crossing can undergo a change in sign of the net energy flux (from southward to northward or vice versa). This can only be accomplished by a shift of the Hadley cell border; increasing or decreasing the energy transport efficiency does not change the sign.

b. Interpreting our GMS results

Our estimate could be reconciled with the nonzero GMS at the ITCZ by forbidding GMS anywhere from dropping below its value at the ITCZ. Despite its imperfect column MSE homogenization, we still expect the intense convection within the ITCZ to communicate surface conditions to the free troposphere more effectively than other regions (Sobel et al. 2002) and thus set the baseline energetic stratification of the tropics. This baseline GMS value is likely model-dependent; see Merlis et al. (2013a) for further discussion of the decomposition of GMS into meridionally varying and uniform components and what sets the GMS value at the ITCZ.

That the actual GMS values drop below the value at the ITCZ near the cell edge does not seriously detract from this modification since the computed changes in this region appear unphysical. As mentioned above, diagnosing the change in GMS as defined in Eq. (A6) in a finite-resolution model becomes difficult near the cell boundary where both its numerator and denominator go to zero, resulting in large unphysical dipoles. Definitions of GMS in terms of vertical velocity and MSE profiles (e.g., Chou and Neelin 2004; Chou et al. 2009) avoid this technical pitfall; however, such measures lose the explicit simple dependence on the MSE and mass fluxes that make Eq. (A6) especially useful for our purposes.

Our neglect of zonal asymmetries is likely problematic. The deep tropical precipitation distribution possesses strong zonal asymmetries throughout the annual cycle (e.g., Hu et al. 2007). Presumably the local stability is nearly zero within local convection zones, but zonally averaging combines these with larger stability values of any nonconvective regions at the same latitude.

Our framework of taking the MSE fluxes as externally imposed and then seeing how they are partitioned between the mass flux and GMS is somewhat arbitrary. Particularly when eddy stresses are important in the momentum balance, the Hadley cell mass flux (and with it GMS) is not free to respond directly to an energetic

TABLE 2. Columns from left to right: month, the latitude of the maximum magnitude of the mass streamfunction (in degrees and denoted ϕ_{\max}) in the control simulation, the northward MSE flux by the Hadley cell at the latitude ϕ_{\max} in the control simulation (in PW), and the fractional changes in the full aerosols simulation from the control at ϕ_{\max} of the Hadley cell energy flux, mass flux, and gross moist stability. The months begin in April rather than January so that the periods when the Southern Hemisphere (April–October) or Northern Hemisphere (November–March) cell is strongest are each continuous within the table.

Month	ϕ_{\max}	$F_{\text{HC}}(\phi_{\max})$	$\frac{\delta F_{\text{HC}}}{F_{\text{HC}}}(\phi_{\max})$	$\frac{\delta \Psi_{\max}}{\Psi_{\max}}(\phi_{\max})$	$\frac{\delta \Delta_{\text{HC}}}{\Delta_{\text{HC}}}(\phi_{\max})$
4	−13.1	−1.12	−0.14	−0.02	−0.11
5	−9.1	−1.68	−0.20	−0.07	−0.14
6	−5.1	−2.21	−0.27	−0.13	−0.17
7	−5.1	−2.71	−0.21	−0.07	−0.14
8	−5.1	−2.65	−0.17	−0.07	−0.11
9	−5.1	−2.19	−0.23	−0.08	−0.17
10	−7.1	−1.12	−0.32	−0.07	−0.26
11	15.2	1.80	0.10	0.09	0.01
12	11.1	2.09	0.21	0.17	0.03
1	9.1	2.53	0.22	0.16	0.05
2	7.1	2.19	0.20	0.15	0.04
3	9.1	1.48	0.28	0.16	0.10

perturbation (e.g., Walker and Schneider 2006). For the solstitial Hadley cell in which eddy stresses are small, the forced mass flux response can be thought of as slaved to the energy and GMS forced responses (Merlis et al. 2013a). But without a simple relationship between anomalous atmospheric energy transport and radiative forcing (due to complicating effects of local feedbacks and ocean transport) and with our GMS scaling being at best qualitatively accurate, constraining the circulation response to forcing remains elusive.

c. Prescribed SSTs

While using prescribed SSTs enables the useful decomposition into mean and spatially varying components, it also prohibits coupling of the atmosphere and ocean responses that are important in the real world. Kang and Held (2012) demonstrate that model Hadley cell responses to extratropical forcing can be sensitive to the details of the imposed SST profiles, which could stem in part from the GMS dependence on SSTs that we have presented. We have not explored the sensitivity of the results to different SST patterns. SST anomalies were attained using a mixed layer ocean–AGCM rather than a fully coupled atmosphere–ocean GCM, and prior studies have demonstrated important differences in the projected SST change with global warming between them (e.g., Xie et al. 2010).

Although both the imposed SST anomalies and the resulting atmospheric responses that we analyze are in equilibrium, nothing precludes our framework from being applied in a transient setting. Given that our GMS theory works best for the spatial pattern cases, it may even do better since presumably SST gradients will be even sharper.

In addition to the simulations already described, Ming and Ramaswamy (2009) also perform an experiment

with the mixed-layer ocean–AM2.1 setup in which both forcing agents are set to their present-day values in the same simulation. Because aerosols counter some of the greenhouse gas–driven mean warming while still imprinting their spatial pattern of NH cooling relative to the SH (annual mean global, NH, and SH mean surface air temperature change are +0.6, +0.2, and +1.3 K, respectively), the responses of this simulation (not shown) are similar to the aerosol spatial pattern prescribed SST simulation.

5. Summary

Using the GFDL AM2.1 AGCM, we have explored how SST anomalies induced by historical anthropogenic emissions of either well-mixed greenhouse gases or aerosols affect the meridional transport of energy by the tropical atmosphere throughout the annual cycle. Complementary simulations in which either the tropical mean SST anomaly is applied at all ocean grid points or the full SST anomalies minus this tropical mean are applied clarify the relative roles of the mean versus the spatial pattern of SSTs, which loosely translate to the thermodynamic and dynamic components of the forced response, respectively.

Greenhouse gases increase the poleward energy transport by eddies, an effect driven by the mean warming but somewhat negated by the polar amplified spatial pattern. Aerosols induce northward energy flux anomalies in the deep tropics via the Hadley cells, owing to their spatial pattern of the NH cooling relative to the SH; this feature is superimposed on a weakening of poleward energy transport driven by the mean cooling.

The mass flux by the Hadley cells is weakened year-round by greenhouse gases, with contributions from

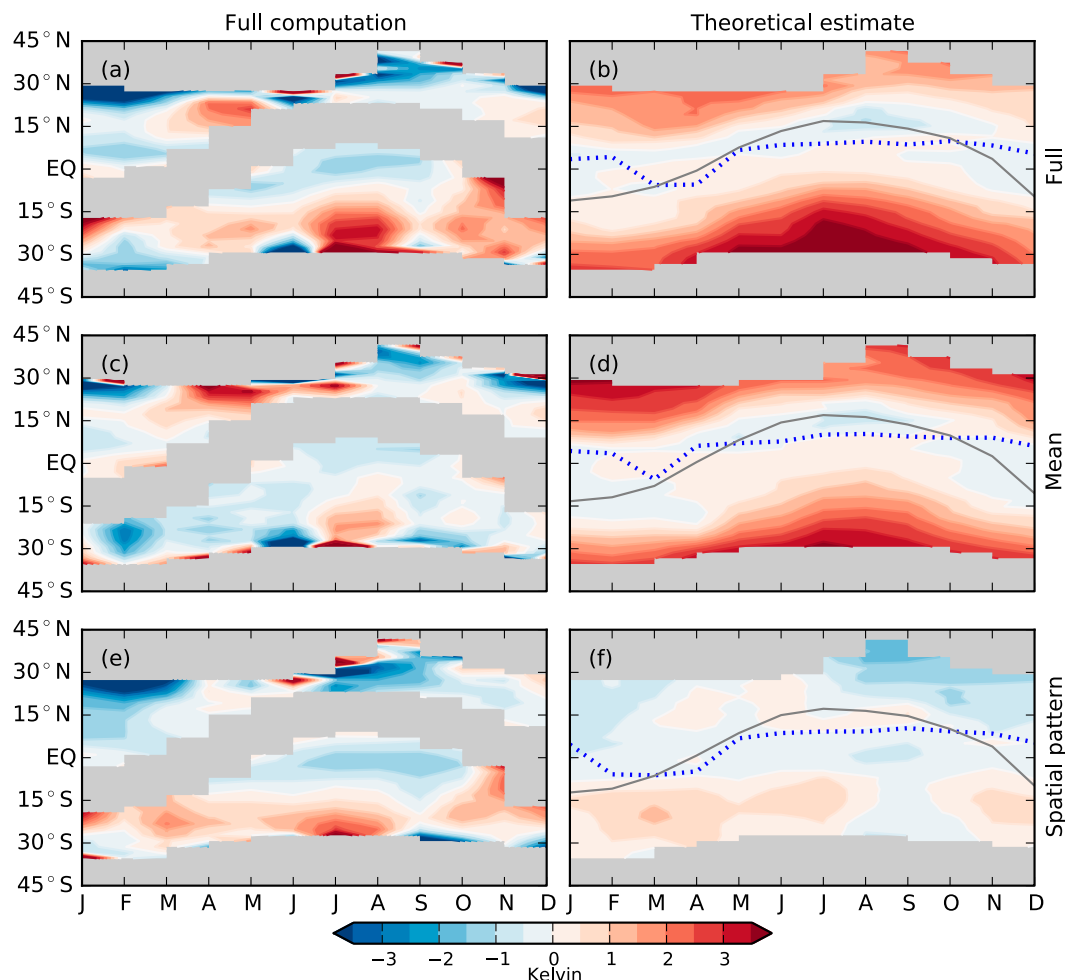


FIG. 10. As in Fig. 9, but for the greenhouse gas simulations.

both the tropical circulation slowdown mediated by the mean warming and the aforementioned weakened energy fluxes due to the polar amplification. The NH-centric aerosol cooling spins up the SH cell and spins down the NH cell; both contribute to the anomalous northward energy flux. For both forcing agents, significant mass flux changes are confined to the latitude range bounded by the seasonal meridional migrations of the Hadley cell interior border.

The Hadley cell gross moist stability—the ratio of the energy and mass fluxes—equivalently measures the difference between upper-level and lower-level moist static energies. By an argument by H01 assuming uniform column moist static energy at the ITCZ and throughout the tropical troposphere aloft, this is approximately equal to the difference between surface MSE values at the given latitude and at the ITCZ. Further assuming thermodynamic scaling of near-surface moisture with temperature implies that uniform warming will enhance, and uniform cooling will reduce, gross moist stability

moving meridionally away from the ITCZ. Overlaid on this mechanism in the aerosol case is a reduction in GMS to the south of the ITCZ and an increase to the north owing to the cooling increasing in magnitude northward. This yields northward energy flux anomalies year round that oppose the imposed NH cooling.

This simple scaling captures the qualitative behavior of the aerosol simulations and the greenhouse gas spatial pattern case but does poorly for the full and mean greenhouse gas components. It predicts weak GMS change near the ITCZ in all cases and, thus, may explain why the mass flux changes are strong at these latitudes, or equivalently why the ITCZ position and the cross-equatorial atmospheric energy transport are so tightly correlated, as prior studies have demonstrated.

Acknowledgments. We thank Leo Donner, Gabriel Lau, Tim Merlis, Dargan Frierson, Aaron Donohoe, Gabe Vecchi, Jonathan Mitchell, and J. David Neelin for insightful comments. Steve Garner and Mike Winton

provided thoughtful reviews of an earlier draft, and comments from three anonymous reviewers greatly improved the paper. S.A.H. was funded first by the NOAA/Princeton University Cooperative Institute for Climate Science and later by the Department of Defense National Defense Science and Engineering Graduate Fellowship.

APPENDIX

Calculation of Meridional Energy Flux, Mass Flux, and Gross Moist Stability

All experiments are integrated on the model's native sigma vertical coordinate system and then interpolated to regular pressure levels as monthly means for analysis. This interpolation produces a small imbalance (a few percent) between the zonal-mean northerly and southerly mass flows that result in somewhat noisy behavior when trying to compute the MSE flux explicitly by integrating MSE times the meridional flow. As such, we introduce an ad hoc correction by defining an adjusted zonal mean meridional wind,

$$[\bar{v}]_{\text{adj}} \equiv [\bar{v}]_+ + [\bar{v}]_- \frac{\{[\bar{v}]_+\}}{\{[\bar{v}]_-\}}, \quad (\text{A1})$$

where $[\bar{v}]_+$ denotes southerly zonal mean wind (i.e., equal to $[\bar{v}]$ if $[\bar{v}] > 0$ and zero otherwise), $[\bar{v}]_-$ denotes northerly wind (defined conversely), and the braces denote a vertical mass-weighted integral, $\{\} \equiv \int dp/g$, where the integral extends over the depth of the column. Note that $\{[\bar{v}]_{\text{adj}}\} \equiv 0$; that is, $[\bar{v}]_{\text{adj}}$ is strictly in mass balance.

The mean meridional circulation component of the meridional MSE flux—that is, the Hadley cell MSE flux $F_{\text{HC}}(\phi)$ —is computed using this mass flux adjusted wind:

$$F_{\text{HC}}(\phi) = \int_{p_{\text{top}}}^{p_{\text{sfc}}} [\bar{m}][\bar{v}]_{\text{adj}} dp/g. \quad (\text{A2})$$

The adjustment removes the interpolation-based noise (not shown), and the resulting MSE flux compares well with the inferred total atmospheric flux (defined below) in the deep tropics where Hadley cells are expected to dominate the energy transport.

The stationary eddy component does not require any mass flux correction:

$$F_{\text{st.edd.}}(\phi) = \int_{p_{\text{top}}}^{p_{\text{sfc}}} [\bar{m}^* \bar{v}^*] dp/g. \quad (\text{A3})$$

We infer the total atmospheric energy transport by assuming steady state and thus relating the total

atmospheric energy flux divergence to the top-of-atmosphere (TOA) and surface flux difference: $\nabla \cdot F_m = Q_{\text{TOA}} - Q_{\text{sfc}}$, where subscripts refer to TOA and surface fluxes, respectively, with downward defined as positive. We then integrate zonally and meridionally:

$$F_{\text{tot}}(\phi) = \int_{-\pi/2}^{\phi} \int_0^{2\pi} (Q_{\text{TOA}} - Q_{\text{sfc}}) a^2 \cos\phi d\lambda d\phi. \quad (\text{A4})$$

The transient eddy term is then taken as the residual of the total minus the time mean (i.e., the Hadley cells plus stationary eddies): $F_{\text{tr.edd.}}(\phi) = F_{\text{tot}}(\phi) - F_{\text{HC}}(\phi) - F_{\text{st.edd.}}(\phi)$. Because the total includes all energy while the explicit calculations include only MSE (neglecting kinetic energy), the transient eddy terms include any resulting residual. But, presumably this residual term is small.

Another concern regarding the MSE flux by the Hadley cells is the vertical extent of the integral. While all of our conceptual analysis invokes tropospheric circulation only, integrating to the model top includes stratospheric flow. Although this circulation is weak and the densities low, large stability values due to the negative lapse rate and large MSE values due to the large geopotential term could result in nonnegligible contributions to the net MSE flux. We test this effect by varying the vertical extent of the MSE flux integral (not shown). While the magnitude of the energy flux tends to decrease slightly by lowering the extent of the integral, the qualitative picture remains the same in either case. Also, since we are taking the transient eddy component as the residual of the total energy flux calculation—which implicitly includes the entire atmosphere—and the time mean component, moving the time mean integrals lower than the model top would lead to the transient eddy term being contaminated by the stratospheric time mean flow. We therefore integrate throughout the depth of the model atmosphere.

For the mass flux Ψ_{max} , we use the signed maximum magnitude value of the Eulerian meridional mass streamfunction at each latitude, where the streamfunction Ψ is defined as

$$\Psi(\phi, p) = 2\pi a \cos\phi \int_0^p [\bar{v}] dp/g. \quad (\text{A5})$$

The mass flux can also be obtained by integrating the adjusted meridional wind $[\bar{v}]_{\text{adj}}$ from the surface to the level where the integral attains its maximum magnitude. The results in either case are nearly identical, so we choose the former, it being more conventional and simpler to calculate.

We calculate the gross moist stability, Δ_{HC} , as the ratio of the energy flux by the Hadley cells, $F_{\text{HC}}(\phi)$ to the mass flux, $\Psi_{\text{max}}(\phi)$:

$$\Delta_{\text{HC}}(\phi) \equiv \frac{\int_{p_{\text{top}}}^{p_{\text{sc}}} [\bar{m}][\bar{v}]_{\text{adj}} dp/g}{\Psi_{\text{max}}}. \quad (\text{A6})$$

Thus defined, Δ_{HC} is positive for a thermally direct circulation such as the Hadley cells. In all plots of Δ_{HC} or its theoretical approximations, we divide by c_p as standard in order to get units of Kelvin.

REFERENCES

- Anderson, J. L., and Coauthors, 2004: The new GFDL global atmosphere and land model AM2-LM2: Evaluation with prescribed SST simulations. *J. Climate*, **17**, 4641–4673, doi:[10.1175/JCLI-3223.1](#).
- Boé, J., A. Hall, and X. Qu, 2009: Current GCMs' unrealistic negative feedback in the Arctic. *J. Climate*, **22**, 4682–4695, doi:[10.1175/2009JCLI2885.1](#).
- Caballero, R., and P. L. Langen, 2005: The dynamic range of poleward energy transport in an atmospheric general circulation model. *Geophys. Res. Lett.*, **32**, L02705, doi:[10.1029/2004GL021581](#).
- Chiang, J. C. H., and A. R. Friedman, 2012: Extratropical cooling, interhemispheric thermal gradients, and tropical climate change. *Annu. Rev. Earth Planet. Sci.*, **40**, 383–412, doi:[10.1146/annurev-earth-042711-105545](#).
- Chou, C., and J. D. Neelin, 2004: Mechanisms of global warming impacts on regional tropical precipitation. *J. Climate*, **17**, 2688–2701, doi:[10.1175/1520-0442\(2004\)017<2688:MOGWIO>2.0.CO;2](#).
- , —, C.-A. Chen, and J.-Y. Tu, 2009: Evaluating the “rich-get-richer” mechanism in tropical precipitation change under global warming. *J. Climate*, **22**, 1982–2005, doi:[10.1175/2008JCLI2471.1](#).
- Delworth, T. L., and Coauthors, 2006: GFDL's CM2 global coupled climate models. Part I: Formulation and simulation characteristics. *J. Climate*, **19**, 643–674, doi:[10.1175/JCLI3629.1](#).
- Dima, I. M., and J. M. Wallace, 2003: On the seasonality of the Hadley cell. *J. Atmos. Sci.*, **60**, 1522–1527, doi:[10.1175/1520-0469\(2003\)060<1522:OTOSO>2.0.CO;2](#).
- Donohoe, A., J. Marshall, D. Ferreira, and D. Mcgee, 2013: The relationship between ITCZ location and cross-equatorial atmospheric heat transport: From the seasonal cycle to the Last Glacial Maximum. *J. Climate*, **26**, 3597–3618, doi:[10.1175/JCLI-D-12-00467.1](#).
- Frierson, D. M. W., 2007: The dynamics of idealized convection schemes and their effect on the zonally averaged tropical circulation. *J. Atmos. Sci.*, **64**, 1959–1976, doi:[10.1175/JAS3935.1](#).
- , and Y.-T. Hwang, 2012: Extratropical influence on ITCZ shifts in slab ocean simulations of global warming. *J. Climate*, **25**, 720–733, doi:[10.1175/JCLI-D-11-00116.1](#).
- , and Coauthors, 2013: Contribution of ocean overturning circulation to tropical rainfall peak in the Northern Hemisphere. *Nat. Geosci.*, **6**, 940–944, doi:[10.1038/ngeo1987](#).
- Held, I. M., 2001: The partitioning of the poleward energy transport between the tropical ocean and atmosphere. *J. Atmos. Sci.*, **58**, 943–948, doi:[10.1175/1520-0469\(2001\)058<0943:TPOTPE>2.0.CO;2](#).
- , and A. Y. Hou, 1980: Nonlinear axially symmetric circulations in a nearly inviscid atmosphere. *J. Atmos. Sci.*, **37**, 515–533, doi:[10.1175/1520-0469\(1980\)037<0515:NASCA>2.0.CO;2](#).
- , and B. J. Hoskins, 1985: Large-scale eddies and the general circulation of the troposphere. *Advances in Geophysics*, Vol. 28, Academic Press, 3–31, doi:[10.1016/S0065-2687\(08\)60218-6](#).
- , and B. J. Soden, 2006: Robust responses of the hydrological cycle to global warming. *J. Climate*, **19**, 5686–5699, doi:[10.1175/JCLI3990.1](#).
- Hu, Y., D. Li, and J. Liu, 2007: Abrupt seasonal variation of the ITCZ and the Hadley circulation. *Geophys. Res. Lett.*, **34**, L18814, doi:[10.1029/2007GL030950](#).
- Hwang, Y.-T., and D. M. W. Frierson, 2010: Increasing atmospheric poleward energy transport with global warming. *Geophys. Res. Lett.*, **37**, L24807, doi:[10.1029/2010GL045440](#).
- Kang, S. M., and I. M. Held, 2012: Tropical precipitation, SSTs and the surface energy budget: A zonally symmetric perspective. *Climate Dyn.*, **38**, 1917–1924, doi:[10.1007/s00382-011-1048-7](#).
- , —, D. M. W. Frierson, and M. Zhao, 2008: The response of the ITCZ to extratropical thermal forcing: Idealized slab-ocean experiments with a GCM. *J. Climate*, **21**, 3521–3532, doi:[10.1175/2007JCLI2146.1](#).
- , D. M. W. Frierson, and I. M. Held, 2009: The tropical response to extratropical thermal forcing in an idealized GCM: The importance of radiative feedbacks and convective parameterization. *J. Atmos. Sci.*, **66**, 2812–2827, doi:[10.1175/2009JAS2924.1](#).
- , C. Deser, and L. M. Polvani, 2013: Uncertainty in climate change projections of the Hadley circulation: The role of internal variability. *J. Climate*, **26**, 7541–7554, doi:[10.1175/JCLI-D-12-00788.1](#).
- Knutson, T. R., and S. Manabe, 1995: Time-mean response over the tropical Pacific to increased CO₂ in a coupled ocean–atmosphere model. *J. Climate*, **8**, 2181–2199, doi:[10.1175/1520-0442\(1995\)008<2181:TMROTT>2.0.CO;2](#).
- Lesins, G., T. J. Duck, and J. R. Drummond, 2012: Surface energy balance framework for arctic amplification of climate change. *J. Climate*, **25**, 8277–8288, doi:[10.1175/JCLI-D-11-00711.1](#).
- Ma, J., and S.-P. Xie, 2013: Regional patterns of sea surface temperature change: A source of uncertainty in future projections of precipitation and atmospheric circulation. *J. Climate*, **26**, 2482–2501, doi:[10.1175/JCLI-D-12-00283.1](#).
- Manabe, S., and R. T. Wetherald, 1975: The effects of doubling the CO₂ concentration on the climate of a general circulation model. *J. Atmos. Sci.*, **32**, 3–15, doi:[10.1175/1520-0469\(1975\)032<0003:TEODTC>2.0.CO;2](#).
- Marshall, J., A. Donohoe, D. Ferreira, and D. McGee, 2014: The ocean's role in setting the mean position of the Inter-Tropical Convergence Zone. *Climate Dyn.*, **42**, 1–13, doi:[10.1007/s00382-013-1767-z](#).
- Merlis, T. M., T. Schneider, S. Bordoni, and I. Eisenman, 2013a: Hadley circulation response to orbital precession. Part I: Aquaplanets. *J. Climate*, **26**, 740–753, doi:[10.1175/JCLI-D-11-00716.1](#).
- , —, —, and —, 2013b: Hadley circulation response to orbital precession. Part II: Subtropical continent. *J. Climate*, **26**, 754–771, doi:[10.1175/JCLI-D-12-00149.1](#).
- , —, —, and —, 2013c: The tropical precipitation response to orbital precession. *J. Climate*, **26**, 2010–2021, doi:[10.1175/JCLI-D-12-00186.1](#).
- Ming, Y., and V. Ramaswamy, 2009: Nonlinear climate and hydrological responses to aerosol effects. *J. Climate*, **22**, 1329–1339, doi:[10.1175/2008JCLI2362.1](#).
- , and —, 2011: A model investigation of aerosol-induced changes in tropical circulation. *J. Climate*, **24**, 5125–5133, doi:[10.1175/2011JCLI4108.1](#).
- , —, L. J. Donner, and V. T. J. Phillips, 2006: A new parameterization of cloud droplet activation applicable to general

- circulation models. *J. Atmos. Sci.*, **63**, 1348–1356, doi:[10.1175/JAS3686.1](https://doi.org/10.1175/JAS3686.1).
- , —, —, —, S. A. Klein, P. A. Ginoux, and L. W. Horowitz, 2007: Modeling the interactions between aerosols and liquid water clouds with a self-consistent cloud scheme in a general circulation model. *J. Atmos. Sci.*, **64**, 1189–1209, doi:[10.1175/JAS3874.1](https://doi.org/10.1175/JAS3874.1).
- Neelin, J. D., and I. M. Held, 1987: Modeling tropical convergence based on the moist static energy budget. *Mon. Wea. Rev.*, **115**, 3–12, doi:[10.1175/1520-0493\(1987\)115<0003:MTCBOT>2.0.CO;2](https://doi.org/10.1175/1520-0493(1987)115<0003:MTCBOT>2.0.CO;2).
- , C. Chou, and H. Su, 2003: Tropical drought regions in global warming and El Niño teleconnections. *Geophys. Res. Lett.*, **30**, 2275, doi:[10.1029/2003GL018625](https://doi.org/10.1029/2003GL018625).
- Peters, M. E., Z. Kuang, and C. C. Walker, 2008: Analysis of atmospheric energy transport in ERA-40 and implications for simple models of the mean tropical circulation. *J. Climate*, **21**, 5229–5241, doi:[10.1175/2008JCLI2073.1](https://doi.org/10.1175/2008JCLI2073.1).
- Privé, N. C., and R. A. Plumb, 2007: Monsoon dynamics with interactive forcing. Part I: Axisymmetric studies. *J. Atmos. Sci.*, **64**, 1417–1430, doi:[10.1175/JAS3916.1](https://doi.org/10.1175/JAS3916.1).
- Reynolds, R. W., N. A. Rayner, T. M. Smith, D. C. Stokes, and W. Wang, 2002: Improved in situ and satellite SST analysis for climate. *J. Climate*, **15**, 1609–1625, doi:[10.1175/1520-0442\(2002\)015<1609:AIHSAS>2.0.CO;2](https://doi.org/10.1175/1520-0442(2002)015<1609:AIHSAS>2.0.CO;2).
- Salmon, R., I. M. Held, J. Fields, and J.-L. Thiffeault, 2001: The general circulation of the atmosphere: 2000 program in geophysical fluid dynamics. Woods Hole Oceanographic Institution Tech. Rep. WHOI-2001-03, 180 pp. [Available online at <http://hdl.handle.net/1912/15>.]
- Sobel, A. H., J. Nilsson, and L. M. Polvani, 2001: The weak temperature gradient approximation and balanced tropical moisture waves. *J. Atmos. Sci.*, **58**, 3650–3665, doi:[10.1175/1520-0469\(2001\)058<3650:TWTGAA>2.0.CO;2](https://doi.org/10.1175/1520-0469(2001)058<3650:TWTGAA>2.0.CO;2).
- , I. M. Held, and C. S. Bretherton, 2002: The ENSO signal in tropical tropospheric temperature. *J. Climate*, **15**, 2702–2706, doi:[10.1175/1520-0442\(2002\)015<2702:TESITT>2.0.CO;2](https://doi.org/10.1175/1520-0442(2002)015<2702:TESITT>2.0.CO;2).
- Trenberth, K. E., and D. P. Stepaniak, 2003: Covariability of components of poleward atmospheric energy transports on seasonal and interannual timescales. *J. Climate*, **16**, 3691–3705, doi:[10.1175/1520-0442\(2003\)016<3691:COCOPA>2.0.CO;2](https://doi.org/10.1175/1520-0442(2003)016<3691:COCOPA>2.0.CO;2).
- Walker, C. C., and T. Schneider, 2006: Eddy influences on Hadley circulations: Simulations with an idealized GCM. *J. Atmos. Sci.*, **63**, 3333–3350, doi:[10.1175/JAS3821.1](https://doi.org/10.1175/JAS3821.1).
- Wyant, M. C., C. S. Bretherton, J. T. Bacmeister, J. T. Kiehl, I. M. Held, M. Zhao, S. A. Klein, and B. J. Soden, 2006: A comparison of low-latitude cloud properties and their response to climate change in three AGCMs sorted into regimes using mid-tropospheric vertical velocity. *Climate Dyn.*, **27**, 261–279, doi:[10.1007/s00382-006-0138-4](https://doi.org/10.1007/s00382-006-0138-4).
- Xie, S.-P., C. Deser, G. A. Vecchi, J. Ma, H. Teng, and A. T. Wittenberg, 2010: Global warming pattern formation: Sea surface temperature and rainfall. *J. Climate*, **23**, 966–986, doi:[10.1175/2009JCLI3329.1](https://doi.org/10.1175/2009JCLI3329.1).
- , B. Lu, and B. Xiang, 2013: Similar spatial patterns of climate responses to aerosol and greenhouse gas changes. *Nat. Geosci.*, **6**, 828–832, doi:[10.1038/ngeo1931](https://doi.org/10.1038/ngeo1931).
- Yoshimori, M., and A. J. Broccoli, 2008: Equilibrium response of an atmosphere–mixed layer ocean model to different radiative forcing agents: Global and zonal mean response. *J. Climate*, **21**, 4399–4423, doi:[10.1175/2008JCLI2172.1](https://doi.org/10.1175/2008JCLI2172.1).

Corrigendum

SPENCER A. HILL

Program in Atmospheric and Oceanic Sciences, Princeton University, Princeton, New Jersey

YI MING AND ISAAC M. HELD

NOAA/Geophysical Fluid Dynamics Laboratory, Princeton, New Jersey

(Manuscript received and in final form 1 July 2016)

In the appendix of [Hill et al. \(2015\)](#), Eqs. (A1), (A2), and (A3) were written incorrectly. For (A1), the operator on the right-hand side should be subtraction, not addition. It should therefore read

$$[\bar{v}]_{\text{adj}} \equiv [\bar{v}]_+ - [\bar{v}]_- \frac{\{[\bar{v}]_+\}}{\{[\bar{v}]_-\}}. \quad (1)$$

For (A2) and (A3), a leading factor of $2\pi a \cos\phi$ is missing on the right-hand side. Therefore, (A2) should appear as

$$F_{\text{HC}}(\phi) = 2\pi a \cos\phi \int_{p_{\text{top}}}^{p_{\text{sc}}} [\bar{m}][\bar{v}]_{\text{adj}} dp/g, \quad (2)$$

and (A3) should appear as


$$F_{\text{st.edd.}}(\phi) = 2\pi a \cos\phi \int_{p_{\text{top}}}^{p_{\text{sc}}} [\bar{m}^* \bar{v}^*] dp/g. \quad (3)$$

The actual computations used the correct form of these equations, and therefore no results are affected.

Acknowledgments. A question from Hao Mingju of Tsinghua University led to the identification of the missing factor in (A2) and (A3) of [Hill et al. \(2015\)](#).

REFERENCE

Hill, S. A., Y. Ming, and I. M. Held, 2015: Mechanisms of forced tropical meridional energy flux change. *J. Climate*, **28**, 1725–1742, doi:[10.1175/JCLI-D-14-00165.1](#).

 Denotes Open Access content.

Corresponding author address: Spencer Hill, NOAA Geophysical Fluid Dynamics Laboratory, 201 Forrestal Rd., Princeton, NJ 08540.
E-mail: spencerh@princeton.edu